20

Sub-wavelength resolution terahertz polarization-sensitive microscopy based on solid immersion effect

© D.R. Il'enkova[1¶], D.D. Rybnikov[1], V.A. Zhelnov[1], A.I. Alekseeva[2], S.L. Shikunov[3], A.V. Kaledin[3], V.I. Polshina[4], A.A. Nebezhev[4], I.V. Reshetov[4], K.I. Zaytsev[1], N.V. Chernomyrdin[1¶¶]

[1] Prokhorov General Physics Institute of the Russian Academy of Sciences
119991 Moscow, Russia
[2] Research Institute of Human Morphology,
117418 Moscow, Russia
[3] Osipyan Institute of Solid State Physics RAS,
142432 Chernogolovka, Russia
[4] I.M. Sechenov First Moscow State Medical University,
119991 Moscow, Russia

[¶]e-mail: iljenckowa.darya@yandex.ru
[¶¶]e-mail: chernik-a@yandex.ru

Received January 09, 2024
Revised January 12, 2024
Accepted March 05, 2024

Terahertz (THz) technologies have many applications in medical diagnostics and therapy. Most are based on effective medium theory, which assumes that biological tissues are optically isotropic and homogeneous over the scales determined by THz wavelengths. Meanwhile, recent studies have shown the possibility of visualizing mesoscale ($\sim \lambda$) tissue inhomogeneities using THz microscopy methods, where λ is the wavelength. In this regard, the problem arises of studying the corresponding effects of scattering and polarization of THz radiation during interaction with biological tissues, for which there are no suitable tools. To solve this problem, a polarization-sensitive reflection-mode THz microscope based on the solid immersion effect has been developed. It uses a silicon hemispherical immersion lens, a metal wire mesh polarizer and analyzer, a backward wave oscillator as a continuous wave source at 0.6 THz ($\lambda = 500\,\mu$m) and a Golay detector. This system makes it possible to study the local polarization-dependent THz response of mesoscale structural elements of tissues with a resolution of up to 0.15λ. Using the developed method, THz images of test media were obtained for two orthogonal states of polarization of incident THz radiation, which made it possible to identify their THz birefringence (structural optical anisotropy). The structural anisotropy of the THz response of porous biomorphic silicon carbide ceramics is considered. Refractive index distributions of freshly excised rat brain were obtained, where the most pronounced THz birefringence is observed in the Corpus callosum, formed by oriented and densely packed axons connecting the cerebral hemispheres. The obtained results show the perspectives of applying THz polarization-sensitive microscopy in biophotonics and medical imaging.

Keywords: terahertz radiation, terahertz microscopy, solid immersion effect, polarization-sensitive microscopy, super-resolution, birefringence, optical anisotropy, brain tissue, Corpus callosum.

DOI: 10.61011/EOS.2024.03.58751.38-24

Introduction

Various methods of terahertz (THz) spectroscopy and imaging have progressed rapidly in recent decades [1,2]. They are currently applied in various branches of science and technology [3,4], including diagnosis of neoplasms [5,6], diabetic foot [7], traumatic injuries [8], burns [9], and tissue vitality [10] and hydration [11]; monitoring of scar healing [12] and transdermal drug delivery [13]; and therapy of malignant and inflammatory diseases [14,15]. Most of these applications are based on effective medium theory, which assumes that biological tissues are optically isotropic and uniform over THz wavelength scales [16,17]. The THz response of such tissues is characterized by relaxation models of complex permittivity and is (largely) determined by the content and state of water in tissues [18,19]. However, recent studies have revealed the possibility of visualization of mesoscale ($\sim \lambda$) tissue inhomogeneities via THz microscopy [3,5,16]. Thus, the problem of study of THz wave scattering in such tissues and the associated polarization effects arises [20].

For example, the authors of [21–24] reported on the use of a polarization-sensitive diffraction-limited THz imaging system for the examination of skin and colon tumors. The aim of these studies was to analyze changes in the polarization of THz radiation occurring during its interaction with tissues. Although the observed depolarization of incident linearly polarized THz radiation is useful for distinguishing healthy tissues from neoplasms, this effect cannot be characterized within the above-mentioned effective medium theory. Owing to the diffraction resolution limit, the mentioned THz polarimetry methods do not provide

accurate data on the driving forces behind the observed depolarization sub-wavelength and mesoscale scatterers in tissues. A multi-configuration THz ellipsometry system, which expands the capabilities of skin tissue analysis using diffraction-limited pulsed THz spectroscopy, was discussed in [25,26]. Combined with a comprehensive model of the interaction of THz waves with the skin, it allows one to quantify the THz response of both the stratum corneum and the epidermis. Specifically, birefringence in the stratum corneum, which is induced by its structure, was revealed.

Various methods of high-resolution near-field THz microscopy were used in [27–33] to visualize sub-wavelength structural elements of tissues, including individual cells. Specifically, our group has designed a THz microscope, which allows for quantitative assessment of the THz optical properties of an object, based on the solid immersion effect for imaging of soft biological tissues with a resolution of 0.15λ. This instrument provides high energy efficiency due to the lack of any sub-wavelength probes or diaphragms in the optical circuit [2,34] and allows one to study the spatial distribution of optical properties and water content over the surface of the examined tissue [35]. It was used to analyze mesoscale inhomogeneities of various tissues (breast, tongue, brain, and pericardium [34–38]); notably, the observed inhomogeneities may induce scattering of THz waves and associated polarization effects [5,20] .

The necessity of studying the effects of interaction of THz radiation with heterogeneous tissues and adapting the theory of radiation transfer to their characterization was demonstrated. A large number of polarization-sensitive systems capable of examining scattering biological tissues in the visible and infrared ranges are available [39–46], but virtually no systems operating in the THz range are known. To solve this problem, a polarization-sensitive microscope based on the solid immersion effect with a resolution of 0.15λ, which utilizes a metal wire mesh polarizer and analyzer, a backward wave oscillator (BWO) acting as a source of continuous radiation at a frequency of 0.6 THz, and a Golay detector, was designed. The developed method was used to obtain THz images of test media for two orthogonal states of polarization of incident THz radiation, which revealed THz birefringence (structural optical anisotropy) of these media. Refractive index distributions of freshly excised rat brain were also plotted to demonstrate the structural optical anisotropy of tissues. The most pronounced THz birefringence was observed in the corpus callosum, which is formed by oriented and densely packed axons connecting the cerebral hemispheres. The obtained results highlight the application potential of polarization-sensitive THz microscopy based on the solid immersion effect in various fields of optics, biophotonics, and medical imaging.

Experimental setup

Figure 1, *a* presents the diagram of the polarization-sensitive THz microscope based on the solid immersion effect, which has been discussed earlier in [47]. This microscope uses a BWO (Prokhorov General Physics Institute, Russian Academy of Sciences) as a source of continuous radiation with a frequency of 0.6 THz ($\lambda = 500\,\mu$m) and a Golay cell as a THz radiation power detector. BWO radiation is modulated at a frequency of 22 Hz using a mechanical modulator for subsequent detection by a synchronous detector. A $1^{\times}$ Kepler telescope with a sub-wavelength metal diaphragm in the intermediate focal plane is used for spatial homogenization of the THz beam (over the aperture).

An original THz optical system based on the solid immersion effect and operating in reflection-mode is the key element of the microscope. It features a wide-aperture aspherical singlet and a hemisphere made of high-resistivity float-zone silicon (HRFZ-Si), which serves to increase spatial resolution [34]. This hemisphere, in turn, is formed by a rigidly fixed hypo-hemispherical lens and a movable flat window on top of which the object is placed. This composite hemisphere design provides an opportunity to image amorphous objects and soft tissues by scanning them with a focused THz beam. These two mechanically independent elements are in contact and form a single optical element: an HRFZ-Si hemisphere with a refractive index of $n_{\mathrm{Si}} = 3.415$. A focal spot of sub-wavelength size is formed at a short distance behind the hemisphere in free space. Figures 1, *b, c* present the results of evaluation of the spatial resolution of the microscope by imaging a metal half-plane with a stepwise change in reflectance for two orthogonal polarizations. The normalized resolution of the microscope reaches $\approx 0.15\lambda$ [34] and depends, to some extent, on the optical properties of the object [35].

The BWO beam is polarized weakly in the vertical direction ($\mathbf{E}_{\mathrm{BWO}}$); the degree of polarization is $\simeq 0.7$. Figures 2, *a, b* show the metal wire mesh polarizer produced by the Prokhorov General Physics Institute of the Russian Academy of Sciences. The metal mesh is stretched over a frame in free space. This mesh is formed by an array of tungsten wires with a diameter and period of 15 and 50 μm, respectively. The polarizer induced linear polarization of the THz beam ($\mathbf{E}_{\mathrm{p}}$) with the electric field oriented at $\pm 45^{\circ}$ relative to the initial BWO polarization ($\mathbf{E}_{\mathrm{BWO}}$). Switching between two orthogonal polarization directions is performed by rotating the polarizer. The intensities of THz radiation incident on the sample and then reaching the detector are almost the same for the $\pm 45^{\circ}$ polarizations, since the corresponding Fresnel losses in interaction with optical elements are equal. This ensures that the obtained THz polarization images have similar signal-to-noise ratio.

Figures 2, *c, d* present the power transmission spectra of the polarizer calculated for a THz field perpendicular and collinear to the metal wires. It is evident that the polarizer is highly efficient.

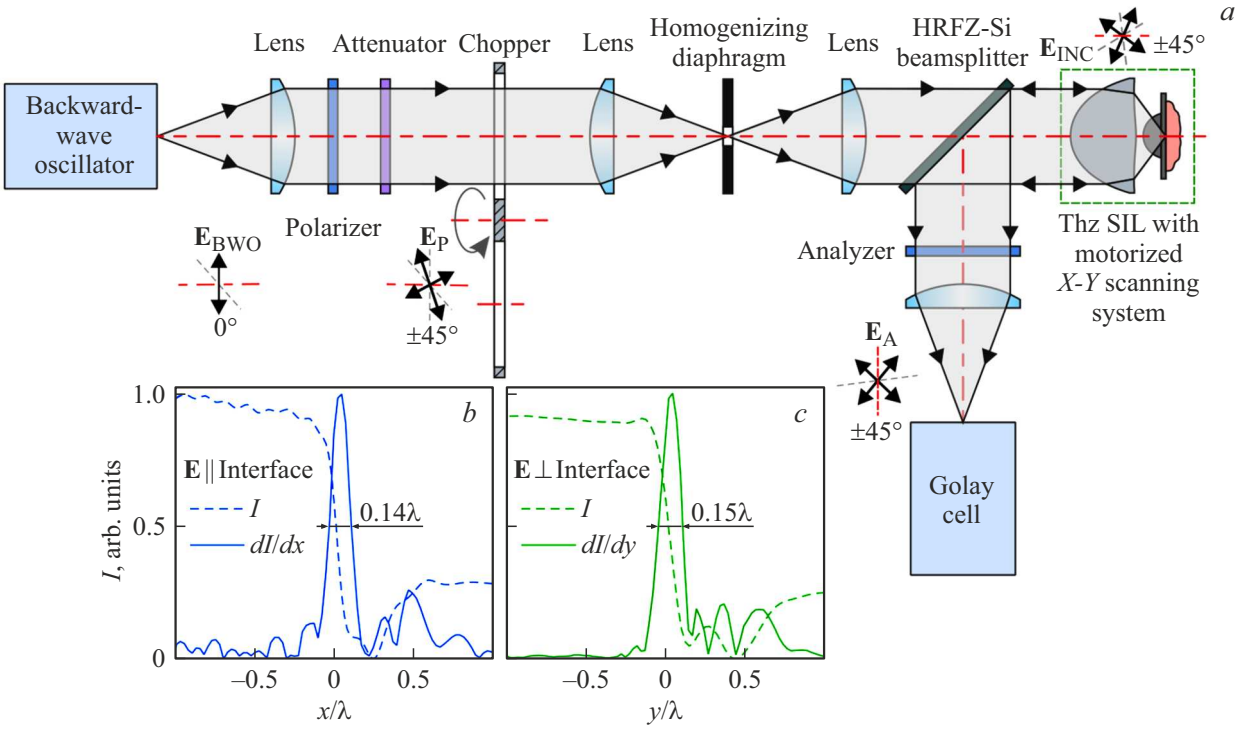

Figure 1. Polarization-sensitive THz microscope based on the solid immersion effect. (*a*) Diagram of the microscope that uses a metal wire mesh polarizer and analyzer, a BWO acting as a source of continuous radiation with a frequency of 0.6 THz ($\lambda = 500\,\mu$m), and a Golay detector. (*b, c*) Results of evaluation of the spatial resolution of the microscope for two orthogonal polarizations, where the normalized resolution reaches 0.15λ.

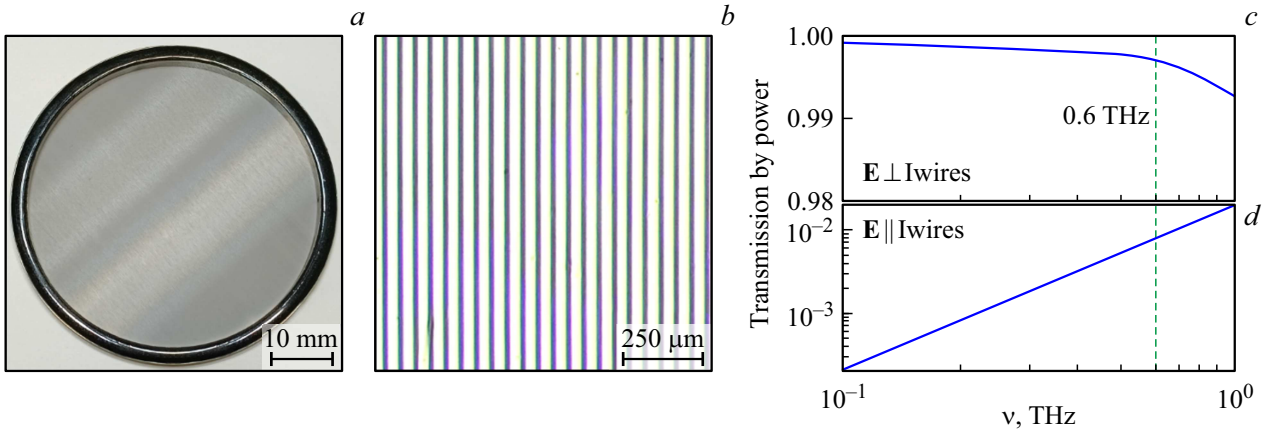

Figure 2. THz wire polarizer: (*a*) photographic image, (*b*) visible-light microscopy data, and (*c, d*) analytically calculated transmission spectra for linearly polarized radiation with its polarization orthogonal and collinear to the wires, respectively.

Figure 1, *a* demonstrates that the analyzer is mounted in front of the detector; its design and characteristics are identical. The analyzer was rotated to switch between ±45° polarization directions for recording co-polarized components of the scattered THz field ($\mathbf{E}_A$). In the discussed microscope design, switching between ±45° polarizations is performed manually by rotating the polarizer and the analyzer. This provides an opportunity to image a stationary object with two orthogonal polarizations of the THz beam (without any displacement or rotation), which is extremely important for imaging of soft biological tissues. This does indeed eliminate any possible tissue shift or deformation and, consequently, the associated THz image distortion.

Although the discussed THz microscope operates at a given BWO frequency of 0.6 THz, the optical system based on the solid immersion effect and the polarizer/analyzer are capable of operating at other THz frequencies (and even broadband operation). Thus, depending on the task at hand, one may combine the designed microscope with other monochromatic or broadband THz radiation sources.

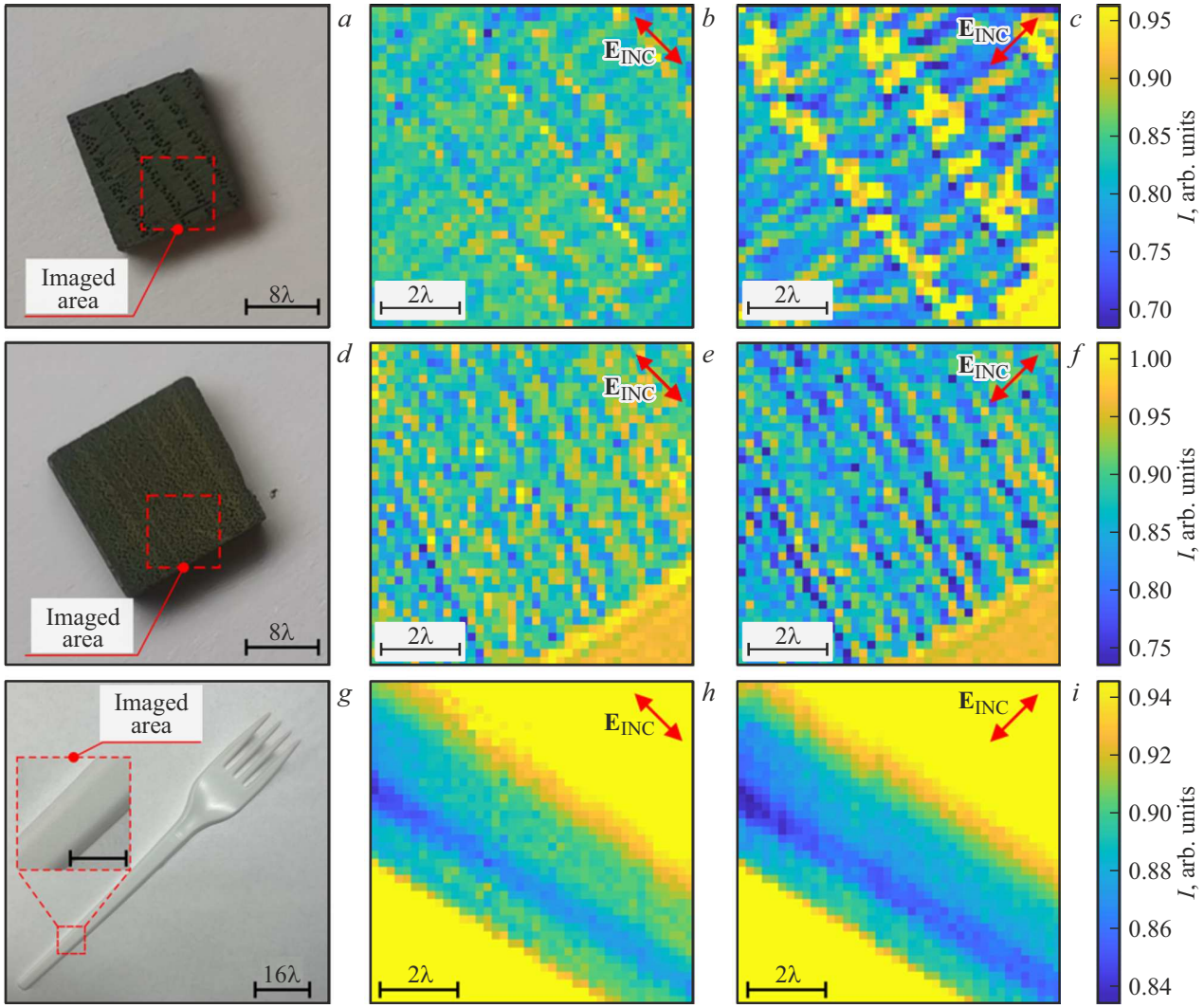

Figure 3. Imaging of test objects with a THz polarization-sensitive microscope based on the solid immersion effect at a frequency of 0.6 THz ($\lambda = 500\,\mu$m). (a–c) Photographic image of a porous biomorphic SiC ceramic material based on oak wood and THz co-polarized images for the cases when $\mathbf{E}_{INC}$ is collinear and orthogonal to the direction of wood fibers and channels. (d–f) and (g–i) Similar data sets for porous biomorphic SiC ceramics based on birch wood and polymer cutlery. The red square denotes the $4 \times 4\,\text{mm}^2$ imaging area.

Polarization-sensitive THz imaging of various test objects

To test the developed THz polarization-sensitive microscope based on the solid immersion effect, we examined test media in which anisotropy of THz optical properties may be observed. Samples of biomorphic silicon carbide ceramics were used as such media [48,49]. The basis of biomorphic silicon carbide ceramics is wood that is subjected to heat treatment in an inert environment to a temperature of 900–1000°C. A porous carbon matrix, which reproduces accurately the original structure of wood, is then formed as a result of pyrolysis. Following interaction of the carbon matrix with silicon melt, a ceramic material is produced. Its primary phases are silicon carbide, which forms a connected microchannel matrix, and residual silicon, which fills the microchannels. A porous biomorphic ceramic material consisting of various β-SiC polytypes is obtained by removing silicon either thermally or chemically.

Figure 3, *a* shows a cross section of porous biomorphic silicon carbide obtained from oak wood. The sample was positioned on the object window in such a way that its microchannels were collinear and orthogonal to the polarization plane of THz radiation. The results of imaging of a $4 \times 4\,\text{mm}^2$ scan area are presented in Figs. 3, *b, c*. Similar measurements were performed for porous biomorphic silicon carbide based on birch wood. Its structure differs significantly from the one of the oak-based sample, since the cross dimensions of channels are smaller; however, birefringence is still observed. Figure 3, *d* shows the photographic image of the sample, and panels (*e*) and (*f*) present the microscopy data for a $4 \times 4\,\text{mm}^2$ region. When the polarization plane of the incident THz wave is orthogonal to the direction of wood fibers, the intensity

of backscattered radiation measured for both samples is higher than the one corresponding to the polarization plane collinear to fibers. This may be attributed to a difference between total cross sections $\sigma_{||}$ and $\sigma_{\perp}$ of scattering of a plane wave off a thin cylindrical object in the Rayleigh approximation with incident wave $\mathbf{E}_{\mathrm{INC}}$ being collinear and orthogonal to the cylinder.

A disposable polymer fork made of polystyrene was another test object. This cutlery is usually made by hot extrusion from a polymer blank. The indicated manufacturing method induces residual stresses in the material after the blank cools, and the directional structure of polymer molecules translates into optical anisotropy of the material. Figures 3, *g*–*i* show the photographic image and two co-polarized THz images of a section of a fork with the direction of polarization of incident wave $\mathbf{E}_{\mathrm{INC}}$ being collinear and orthogonal to the presumed direction of extrusion. It can be seen that when $\mathbf{E}_{\mathrm{INC}}$ is orthogonal to the extrusion direction, the intensity of backscattered radiation is lower than the one corresponding to $\mathbf{E}_{\mathrm{INC}}$ collinear to the extrusion direction.

Thus, the feasibility of application of the developed THz microscopy system based on the solid immersion effect for polarization-sensitive measurements of various types of objects was demonstrated.

THz microscopy of rat brain tissue

In work [47] for the first time have been used to observe polarization-sensitive THz microscopy to observe structural anisotropy (birefringence) of freshly excised rat brain tissues *ex vivo*. This common phenomenon has been observed numerous times in the visible and infrared ranges for various fibrous tissues formed by densely packed and oriented cylindrical/elliptical scatterers [50]. For example, this effect was noted in the infrared range in the corpus callosum that is formed by bundles of axons connecting the cerebral hemispheres [51]. However, birefringence in the THz range is poorly studied and was observed only for the stratum corneum of the skin via THz ellipsometry [52]. To demonstrate tissue birefringence in the THz range with sub-wavelength resolution, we used the developed THz microscope to examine a freshly excised intact rat brain (in particular, the corpus callosum) *ex vivo*.

A freshly excised frontal section of the brain was positioned on the HRFZ-Si microscope window (Fig. 1, *a*) so that the side of the section was adjacent to the window. Its reverse side was covered with a thin polyethylene film to prevent hydration/dehydration of the tissue and suppress the associated distortion of the measured THz response. Following measurements, the tissue sample was fixed (for 48 h) in a 4% paraformaldehyde solution and embedded into a paraffin block. Tissue sections 5 μm in thickness were stained with hematoxylin and eosin (H&E); their histological examination allowed us to identify and mark brain structures. Figures 4,*a, b* show the photographic image of a freshly excised intact rat brain and the corresponding H&E-stained histological section.

In the course of THz imaging, the polarization of incident THz beam $\mathbf{E}_{\mathrm{INC}}$ was first set collinear and then orthogonal to the bundle of axons in the corpus callosum, which lie in the image plane. THz images of a brain area $10 \times 10\,\mathrm{mm}^2$ in size were recorded. A quantitative assessment of the spatial distribution (over the image area) of refractive index of tissue n at a frequency of 0.6 THz was performed for two orthogonal polarizations (Figs. 4, *c, d*) by solving the inverse problem of THz microscopy based on the solid immersion effect, which was discussed in detail in [35]. The developed THz microscope allows one to study the response of superficial tissues only, which is due to the limited depth of field [34] and the shallow depth of penetration of THz waves into tissues [19]; both parameters are on the order of $\approx 100\,\mu$m. It is evident that the THz images and n distributions for two orthogonal polarizations differ significantly. Two areas of interest are highlighted in the histological section stained with H&E (Fig. 4, *b*): (I) corpus callosum and (II) cortex.

Figures 4, *e, f* show the normalized statistical distributions of refractive index of tissue $p(n)$ for these regions. As expected, panel (*e*) reveals a fairly high birefringence for corpus callosum (I), where n is higher for $\mathbf{E}_{\mathrm{INC}}$ polarized along the axons. In turn, cerebral cortex (II) in panel (*f*) exhibits virtually no birefringence, since its morphology is isotropic on the THz wavelength scale. A less pronounced anisotropy is observed for other brain regions (white and gray matter included) in Figs. 4, *c, d*, but a detailed analysis of their THz responses is beyond the scope of the present study.

Discussion

Thus, the sensitivity of THz polarization-sensitive microscopy to local ordering and orientation of the object structure was demonstrated. However, an object needs to be probed with a large number of polarizations at different orientations relative to the object and different incidence angles to increase the sensitivity of this approach. The cross-polarized component of the scattered THz field may also be a source of useful information [22] complementing co-polarized data. This approach may be applied in the study of THz responses of biological tissues that, in certain cases, have structural elements comparable in size to those of silicon carbide. Terahertz birefringence may be observed in various biological tissues of humans and animals (such as fibrous tissues of muscles and tendons, capillaries, and veins) [34,36] or even plants (veins and capillaries) [34,53].

Polarization-sensitive THz microscopy based on the solid immersion effect has application potential in various fields of medical imaging, including ophthalmology (study of corneal pathologies [54]), oncological diagnostics (diagnosis of melanoma [55], basal cell carcinoma [56], lung cancer [57],

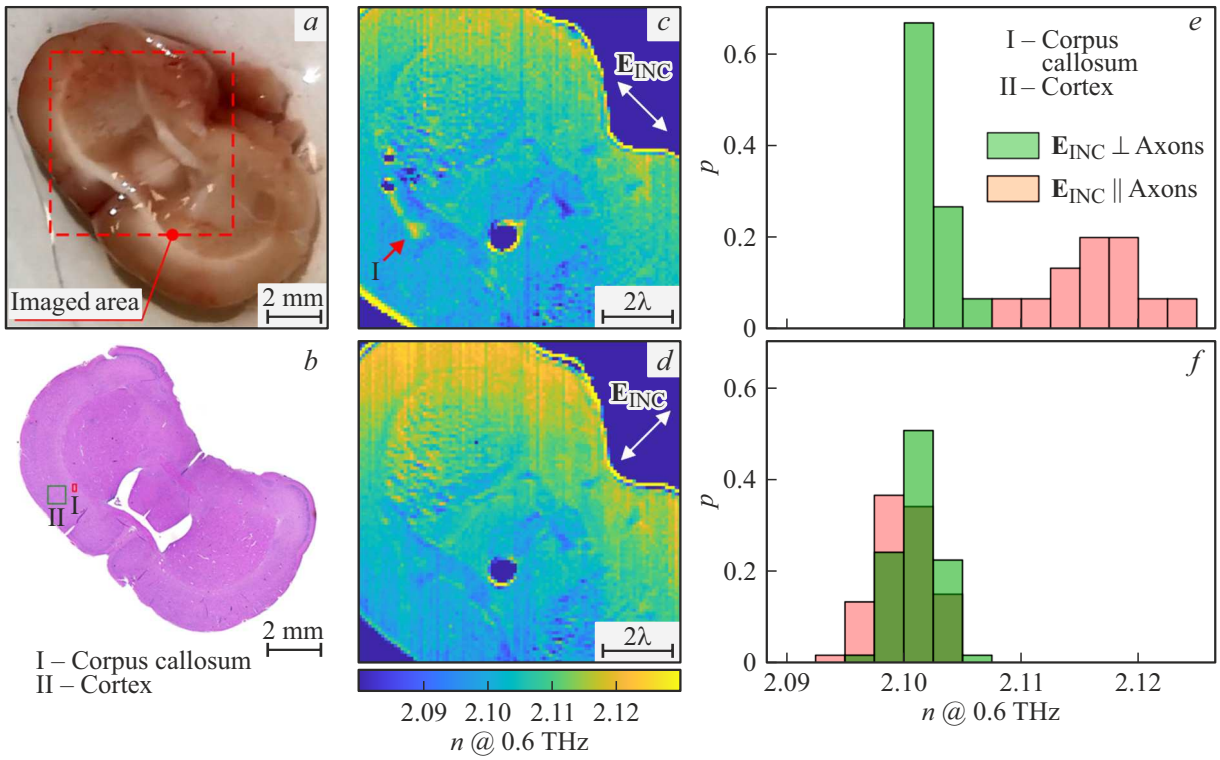

Figure 4. Polarization-sensitive microscopy based on the solid immersion effect of a rat brain *ex vivo* at a frequency of 0.6 THz ($\lambda = 500\,\mu$m). (*a, b*) Photographic image and histological examination of the rat brain with H&E staining. Indicated are the imaged area and two areas of interest: corpus callosum (I) and cortex (II). (*c, d*) Spatial distribution of THz refractive index n in the cases when THz field $\mathbf{E}_{\text{INC}}$ polarized linearly in the image plane is collinear and orthogonal to axons in the corpus callosum. (*e,f*) Histograms of distribution of THz refractive indices in brain regions I and II, respectively; (*e*) reveals significant THz birefringence of corpus callosum. The figure was taken from study [47] that was published under the Creative Commons Attribution 4.0 International License (CC BY).

brain tumors [16], etc.), study of cardiovascular diseases (disorders of the urinary wall bladder [58], diabetic foot [7]), neuroscience, etc.

The efficacy of this method may be increased further through the use of the Mueller matrix formalism [59,60], which utilizes a 4×4 matrix to characterize the transformation of polarization of an electromagnetic wave in the course of its interaction with a scattering medium. The decomposition of the Mueller matrix allows one to estimate such polarization parameters of the medium as optical rotation and linear phase shift [61,62]. Various instrumental implementations of polarization microscopy in the visible and infrared ranges have been proposed. These include the classical implementation (36 measurements with various combinations of a polarizer and an analyzer are needed to evaluate a 4×4 Mueller matrix) and the rotating retarder approach, which reduces the number of measurements to 24 [63]. Given the large number of images that must be obtained for Mueller matrix analysis, a need arises to improve the performance of the microscopy system (raise its operating speed and sensitivity).

• First, the acquisition time of the THz microscope based on the solid immersion effect should be optimized by using a faster pyroelectric detector and a raster scanning system with fast stepper motors. This may reduce the time of a single scan to 2–3 min, which is important for Mueller polarimetry that requires dozens of polarimetric images.

• Second, the Mueller matrix evaluation requires THz beams with both linear and elliptical polarizations. One may produce such a set of linear and elliptical polarizations of a THz beam either using classical polarization converters based on THz materials with birefringence (crystalline quartz, sapphire, etc.) or opt for new approaches based on various physical effects in graphene [64], vanadium dioxide [65], metal wire gratings [66], multilayer metamaterials [67], 3D printed conductive polymer structures [68], and separators based on parallel plates [69].

• Third, Mueller matrix polarimetry normally involves the interaction of low-aperture beams with a sample, while THz microscopy based on the solid immersion effect uses wide-aperture beams to excite evanescent waves at the interface between a silicon lens and an object. To combine Mueller matrix polarimetry with THz microscopy based on the solid immersion effect, one needs to take into account the wide beam aperture and modify the underlying physical models accordingly.

The advantages of polarization measurements in the THz range over experiments in other spectral regions are also

worth emphasizing. First, the studied spectral characteristics of a substance (absorption lines or bands) vary from one spectral range to another due to the difference in energy of radiation quanta and, consequently, in mechanisms of interaction of electromagnetic waves with matter. Second, the polarization effects under study are associated with scattering of electromagnetic waves and are thus governed by the relation between the wavelength and sizes/shapes of structural elements of the object. Therefore, polarization measurements in different spectral ranges (including the terahertz one) probe the influence of object inhomogeneities of various scales. Thus, THz spectroscopy and microscopy provide unique information about the object under study, which complements, to some extent, spectroscopy and imaging data from other bands. In general, to gain a deeper understanding of the mechanisms of interaction of electromagnetic radiation with an object and choose the optimum spectral range for a particular application (e.g., non-destructive quality control or medical diagnostics), it is better to perform broadband measurements first and then choose certain optimum spectral ranges and wavelengths.

Polarization reflection and transmission microscopy and endoscopy with optical fibers are used widely in the visible and infrared ranges [45]. These approaches may be implemented in the THz range to reveal the polarization effects of interaction of THz waves with an object. Maximization of the information content of images provided by polarization-sensitive THz microscopy based on the solid immersion effect, development of new methods for data collection and analysis, and examination of their applications in biomedicine are promising directions for further research.

Conclusion

A polarization-sensitive THz microscope based on the solid immersion effect was designed. The microscope operates at a frequency of 0.6 THz with a resolution up to 0.15λ and allows one to examine the spatial distribution of anisotropic THz optical properties of an object. The applicability of the new method in studies of the anisotropic THz response of various objects with sub-wavelength resolution was demonstrated. Terahertz birefringence of a freshly excised intact rat brain *ex vivo* was revealed.The most pronounced anisotropy was observed in the corpus callosum (a bundle of densely packed and oriented axons connecting the cerebral hemispheres). The obtained results highlight the application prospects of polarization-sensitive THz microscopy in optics and biophotonics.

Compliance with ethical standards

Experiments with laboratory animals were carried out at the Research Institute of Human Morphology (Moscow, Russia). Animals were kept under standard vivarium conditions in accordance with Sanitary Rules for the Design, Outfitting, and Maintenance of Experimental Biological Clinics (Vivariums) SP N 1045-73 approved by the Ministry of Health of the Union of Soviet Socialist Republics on July 6, 1973. Specifically, rats were kept on a bedding material in individual R-1 cages 460 × 300 × 160 mm in size with steel lattice covers with a feeding recess. Animals received water (satisfying the requirements of GOST 2874-82 „Drinking Water“) ad libitum. Animals received „PK-120-1760“ complete feed ad libitum. Sawdust was used as bedding with daily changes during inspection and massometry. Animals were kept under natural light conditions at a temperature of 19−21°C and a relative humidity of 60−75%. The management of animals, all manipulations with them, and their withdrawal from the experiment were in accordance with the Principles of Good Laboratory Practice in the Russian Federation approved by the Ministry of Health of the Russian Federation (order No. 267 dated June 19, 2003) and the Rules of Bioethics approved by the European Convention for the Protection of Vertebrate Animals used for Experimental and Other Scientific Purposes (Strasbourg, 1986).

Acknowledgments

Funding

This study was supported by the Russian Science Foundation, project No. 22-79-10099.

Conflict of interest

The authors declare that they have no conflict of interest.

References

[1] H. Guerboukha, K. Nallappan, M. Skorobogatiy. Adv. Opt. Photon., **10** (4), 843?938 (2018). DOI: 10.1364/AOP.10.000843
[2] N.V. Chernomyrdin, M. Skorobogatiy, D.S. Ponomarev, V.V. Bukin, V.V. Tuchin, K.I. Zaytsev. Appl. Phys. Lett., **120** (11), 110501 (2022). DOI: 10.1063/5.0085906
[3] O.A. Smolyanskaya, N.V. Chernomyrdin, A.A. Konovko, K.I. Zaytsev, I.A. Ozheredov, O.P. Cherkasova, M.M. Nazarov, J.-P. Guillet, S.A. Kozlov, Yu. V Kistenev, J.-L. Coutaz, P. Mounaix, V.L. Vaks, J.-H. Son, H. Cheon, V.P. Wallace, Yu. Feldman, I. Popov, A.N. Yaroslavsky, A.P. Shkurinov, V.V. Tuchin. Prog. Quantum. Electron., **62**, 1−77 (2018). DOI: 10.1016/j.pquantelec.2018.10.001
[4] Z. Yan, L.-G. Zhu, K. Meng, W. Huang, Q. Shi. Trends Biotechnol, **40** (7), 816−830 (2022). DOI: 10.1016/j.tibtech.2021.12.002
[5] K. Zaytsev, I. Dolganova, N. Chernomyrdin, G. Katyba, A. Gavdush, O. Cherkasova, G. Komandin, M. Shchedrina, A. Khodan, D. Ponomarev, I. Reshetov, V.E. Karasik, M. Skorobogatiy, V. Kurlov, V. Tuchin. J. Opt., **22**, 13001 (2020). DOI: 10.1088/2040-8986/ab4dc3
[6] H. Lindley-Hatcher, R.I. Stantchev, X. Chen, A.I. Hernandez-Serrano, J. Hardwicke, E. Pickwell-MacPherson. Appl. Phys. Lett., **118** (23), 230501 (2021). DOI: 10.1063/5.0055259

[7] G.G. Hernandez-Cardoso, L.F. Amador-Medina, G. Gutierrez-Torres, E.S. Reyes-Reyes, C.A.B. Martínez, C.C. Espinoza, J.A. Cruz, I. Salas-Gutierrez, B.O. Murillo-Ortiz, E. Castro-Camus. Sci. Rep., **12**, 3110 (2022). DOI: 10.1038/s41598-022-06996-w
[8] H. Zhao, Y. Wang, L. Chen, J. Shi, K. Ma, L. Tang, D. Xu, J. Yao, H. Feng, T. Chen. J. Biomed. Opt., **23** (3), 36015 (2018). DOI: 10.1117/1.JBO.23.3.036015
[9] N. Bajwa, S. Sung, D.B. Ennis, M.C. Fishbein, B.N. Nowroozi, D. Ruan, A. Maccabi, J. Alger, M.A.St. John, W.S. Grundfest, Z.D. Taylor. IEEE Trans. Biomed. Eng., **64** (11), 2682–2694 (2017). DOI: 10.1109/TBME.2017.2658439
[10] N. Bajwa, J. Au, R. Jarrahy, S. Sung, M. Fishbein, D. Riopelle, D. Ennis, T. Aghaloo, M. John, W. Grundfest, Z. Taylor. Biomed. Opt. Express, **8**, 460 (2017). DOI: 10.1364/BOE.8.000460
[11] O.A. Smolyanskaya, I.J. Schelkanova, M.S. Kulya, E.L. Odlyanitskiy, I.S. Goryachev, A.N. Tcypkin, Ya.V. Grachev, Ya.G. Toropova, V.V Tuchin. Biomed. Opt. Express, **9** (3), 1198–1215 (2018). DOI: 10.1364/BOE.9.001198
[12] X. Ding, G. Costa, A.I. Hernandez-Serrano, R.I. Stantchev, G. Nurumbetov, D.M. Haddleton, E. Pickwell-MacPherson. Biomed. Opt. Express, **14** (3), 1146–1158 (2023). DOI: 10.1364/BOE.473097
[13] J. Wang, Q. Sun, R.I. Stantchev, T.-W. Chiu, A.T. Ahuja, E. Pickwell-MacPherson. Biomed. Opt. Express, **10** (7), 3584–3590 (2019). DOI: 10.1364/BOE.10.003584
[14] O.P. Cherkasova, D.S. Serdyukov, E.F. Nemova, A.S. Ratushnyak, A.S. Kucheryavenko, I.N. Dolganova, G. Xu, M. Skorobogatiy, I.V Reshetov, P.S. Timashev, I.E. Spektor, K.I. Zaytsev, V.V Tuchin. J. Biomed. Opt., **26** (9), 90902 (2021). DOI: 10.1117/1.JBO.26.9.090902
[15] H. Cheon, J.K. Hur, W. Hwang, H.-J. Yang, J.-H. Son. Sci. Rep., **13**, 4930 (2023). DOI: 10.1038/s41598-023-31828-w
[16] N.V. Chernomyrdin, G.R. Musina, P.V Nikitin, I.N. Dolganova, A.S. Kucheryavenko, A.I. Alekseeva, Y. Wang, D. Xu, Q. Shi, V.V Tuchin, K.I. Zaytsev. Opto. Electron. Adv., **6** (5), 220071 (2023). DOI: 10.29026/oea.2023.220071
[17] E. Pickwell, B.E. Cole, A.J. Fitzgerald, V.P. Wallace, M. Pepper. Appl. Phys. Lett., **84** (12), 2190?2192 (2004). DOI: 10.1063/1.1688448
[18] S. Yamaguchi, Y. Fukushi, O. Kubota, T. Itsuji, T. Ouchi, S. Yamamoto. Phys. Med. Biol., **61** (18), 6808 (2016). DOI: 10.1088/0031-9155/61/18/6808
[19] A.A. Gavdush, N.V. Chernomyrdin, G.A. Komandin, I.N. Dolganova, P.V. Nikitin, G.R. Musina, G.M. Katyba, A.S. Kucheryavenko, I.V. Reshetov, A.A. Potapov, V.V. Tuchin, K.I. Zaytsev. Biomed. Opt. Express, **12** (1), 69–83 (2021). DOI: 10.1364/BOE.411025
[20] A.S. Kucheryavenko, I.N. Dolganova, A.A. Zhokhov, V.M. Masalov, G.R. Musina, V.V. Tuchin, N.V. Chernomyrdin, A.A. Gavdush, D.R. Il'enkova, S.V. Garnov, K.I. Zaytsev. Phys. Rev. Appl., **20** (5), 054050 (2023). DOI: 10.1103/PhysRevApplied.20.054050
[21] P. Doradla, K. Alavi, C.S. Joseph, R.H. Giles. J. Biomed. Opt., **18** (9), 90504 (2013). DOI: 10.1117/1.JBO.18.9.090504
[22] C.S. Joseph, R. Patel, V.A. Neel, R.H. Giles, A.N. Yaroslavsky. J. Biophotonics, **7** (5), 295–303 (2014). DOI: 10.1002/jbio.201200111
[23] B. Fan, V.A. Neel, A.N. Yaroslavsky. Las. Surg. Med., **49** (5), 319–326 (2017). DOI: 10.1002/lsm.22552
[24] A. Yaroslavsky, C. Joseph, R. Patel, A. Muzikansky, V. Neel, R. Giles. J. Biomed. Photon. Eng., **3** (1), 3170 (2017). DOI: 10.18287/JBPE17.03.010301.
[25] X. Chen, Q. Sun, J. Wang, H. Lindley-Hatcher, E. Pickwell-MacPherson. Adv. Photon. Res., **2** (1), 2000024 (2021). DOI: 10.1002/adpr.202000024
[26] X. Chen, E. Pickwell-MacPherson. APL Photon., **7** (7), 71101 (2022). DOI: 10.1063/5.0094056
[27] R. D' Antuono, J.W. Bowen. J. Microsc., **288** (3), 207–217 (2022). DOI: 10.1111/jmi.13132
[28] U. Schade, K. Holldack, P. Kuske, G. Wustefeld, H.-W. Hubers. Appl. Phys. Lett., **84** (8), 1422–1424 (2004). DOI: 10.1063/1.1650034
[29] C.-M. Chiu, H.-W. Chen, Y.-R. Huang, Y.-J. Hwang, W.-J. Lee, H.-Y. Huang, C.-K. Sun. Opt. Lett., **34** (7), 1084–1086 (2009). DOI: 10.1364/OL.34.001084
[30] Z. Li, Z. Zang, J. Wang, X. Lu, Z. Yang, H. Wang, H.-L. Cui, S. Yan. IEEE Trans. Terahertz Sci. Technol., **12** (5), 457–463 (2022). DOI: 10.1109/TTHZ.2022.3170010
[31] K. Okada, K. Serita, Q. Cassar, H. Murakami, G. MacGrogan, J.-P. Guillet, P. Mounaix, M. Tonouchi. J. Phys. Photon., **2** (4), 44008 (2020). DOI: 10.1088/2515-7647/abbcda
[32] Z. Li, S. Yan, Z. Zang, G. Geng, Z. Yang, J. Li, L. Wang, C. Yao, H.-L. Cui, C. Chang, H. Wang. Cell Prolif., **53** (4), e12788 (2020). DOI: 10.1111/cpr.12788
[33] K. Okada, Q. Cassar, H. Murakami, G. MacGrogan, J.-P. Guillet, P. Mounaix, M. Tonouchi, K. Serita. Opt. Contin., **1** (3), 527–537 (2022). DOI: 10.1364/OPTCON.448444
[34] N.V. Chernomyrdin, A.S. Kucheryavenko, G.S. Kolontaeva, G.M. Katyba, I.N. Dolganova, P.A. Karalkin, D.S. Ponomarev, V.N. Kurlov, I.V. Reshetov, M. Skorobogatiy, V.V. Tuchin, K.I. Zaytsev. Appl. Phys. Lett., **113** (11), 111102 (2018). DOI: 10.1063/1.5045480
[35] N.V. Chernomyrdin, M. Skorobogatiy, A.A. Gavdush, G.R. Musina, G.M. Katyba, G.A. Komandin, A.M. Khorokhorov, I.E. Spektor, V.V. Tuchin, K.I. Zaytsev. Optica, **8** (11), 1471–1480 (2021). DOI: 10.1364/OPTICA.439286
[36] N.V Chernomyrdin, A.S. Kucheryavenko, E.N. Rimskaya, I.N. Dolganova, V.A. Zhelnov, P.A. Karalkin, A.A. Gryadunova, I.V. Reshetov, D.V. Lavrukhin, D.S. Ponomarev, V.E. Karasik, K.I. Zaytsev. Opt. Spectrosc., **126** (5), 560–567 (2019). DOI: 10.1134/S0030400X19050059
[37] A.S. Kucheryavenko, N.V. Chernomyrdin, A.A. Gavdush, A.I. Alekseeva, P.V. Nikitin, I.N. Dolganova, P.A. Karalkin, A.S. Khalansky, I.E. Spektor, M. Skorobogatiy, V.V. Tuchin, K.I. Zaytsev. Biomed. Opt. Express, **12** (8), 5272–5289 (2021). DOI: 10.1364/BOE.432758
[38] G.R. Musina, N.V Chernomyrdin, E.R. Gafarova, A.A. Gavdush, A.J. Shpichka, G.A. Komandin, V.B. Anzin, E.A. Grebenik, M.V Kravchik, E.V. Istranova, I.N. Dolganova, K.I. Zaytsev, P.S. Timashev. Biomed. Opt. Express, **12** (9), 5368 (2021). DOI: 10.1364/BOE.433216
[39] V.V Tuchin. J. Biomed. Opt., **21** (7), 71114 (2016). DOI: 10.1117/1.JBO.21.7.071114
[40] A.N. Bashkatov, K. V Berezin, K.N. Dvoretskiy, M.L. Chernavina, E.A. Genina, V.D. Genin, V.I. Kochubey, E.N. Lazareva, A.B. Pravdin, M.E. Shvachkina, P.A. Timoshina, D.K. Tuchina, D.D. Yakovlev, D.A. Yakovlev, I.Y. Yanina, O.S. Zhernovaya, V.V Tuchin. J. Biomed. Opt., **23** (9), 91416 (2018). DOI: 10.1117/1.JBO.23.9.091416
[41] S.-Y. Lu, R.A. Chipman. J. Opt. Soc. Am., **13** (5), 1106–1113 (1996). DOI: 10.1364/JOSAA.13.001106
[42] R. Ossikovski. J. Opt. Soc. Am., **25** (2), 473–482 (2008). DOI: 10.1364/JOSAA.25.000473
[43] R. Ossikovski. J. Opt. Soc. Am., **26** (5), 1109–1118 (2009). DOI: 10.1364/JOSAA.26.001109

[44] O. Arteaga, A. Canillas. J. Opt. Soc. Am., **26** (4), 783–793 (2009). DOI: 10.1364/JOSAA.26.000783
[45] S. Manhas, J. Vizet, S. Deby, J.-C. Vanel, P. Boito, M. Verdier, A. De Martino, D. Pagnoux. Opt. Express, **23** (3), 3047 (2015). DOI: 10.1364/OE.23.003047
[46] D. Vala, M. Micica, D. Cvejn, K. Postava. RSC Adv., **13** (10), 6582–6592 (2023). DOI: 10.1039/D3RA00101F
[47] N.V. Chernomyrdin, D.R. Il'enkova, V.A. Zhelnov, A.I. Alekseeva, A.A. Gavdush, G.R. Musina, P.V. Nikitin, A.S. Kucheryavenko, I.N. Dolganova, I.E. Spektor, V.V. Tuchin, K.I. Zaytsev. Sci. Rep., **13** (1), 16596 (2023). DOI: 10.1038/s41598-023-43857-6
[48] P. Greil, T. Lifka, A. Kaindl. J. Eur. Ceram. Soc., **18** (14), 1961–1973 (1998). DOI: 10.1016/S0955-2219(98)00156-3
[49] A.E. Ershov, S.L. Shikunov, V.N. Kurlov. Tech. Phys., **62** (6), 903–910 (2017). DOI: 10.1134/S1063784217060093
[50] C.R. Simovski, P.A. Belov, A.V. Atrashchenko, Y.S. Kivshar. Adv. Mater., **24** (13), 4229–4248 (2012). DOI: 10.1002/adma.201200931
[51] H. van de Hulst. Wiley. *Light Scattering by Small Particles* (John Wiley and Sons, New York, 1957). DOI: 10.1063/1.3060205
[52] X. Chen, Q. Sun, J. Wang, H. Lindley-Hatcher, E. Pickwell-MacPherson. Adv. Photon. Res., **2** (1), 2000024 (2021). DOI: 10.1002/adpr.202000024
[53] A.V. Shchepetilnikov, A.M. Zarezin, V.M. Muravev, P.A. Gusikhin, I.V. Kukushkin. Opt. Eng., **59** (6), 61617 (2020). DOI: 10.1117/1.OE.59.6.061617
[54] E. Fariza, T. O'Day, A.E. Jalkh, A. Medina. Arch. Ophthalmol., **107** (4), 608–610 (1989). DOI: 10.1001/archopht.1989.01070010622044
[55] Z. Tannous, M. Al-Arashi, S. Shah, A.N. Yaroslavsky. Las. Surg. Med., **41** (1), 10–16 (2009). DOI: 10.1002/lsm.20736
[56] I. Ahmad, M. Ahmad, K. Khan, M. Ikram. Photodiagnosis Photodyn. Ther., **14**, 134–141 (2016). DOI: 10.1016/j.pdpdt.2016.04.004
[57] S. Shrestha, A. Deshpande, T. Farrahi, T. Cambria, T. Quang, J. Majeski, Y. Na, M. Zervakis, G. Livanos, G.C. Giakos. Biomed. Signal. Process. Control, **40**, 505–518 (2018). DOI: 10.1016/j.bspc.2017.05.009
[58] S. Alali, K.J. Aitken, A. Schr?der, A. Gribble, D.J. Bagli, I.A. Vitkin. Biomed. Opt. Express, **5** (2), 621–629 (2014). DOI: 10.1364/BOE.5.000621
[59] H. Mueller, F. Melsheimer. Zeitschrift Für Technische Physik, **22**, 53–63 (1941).
[60] J.L. Pezzaniti, R.A. Chipman. Opt. Eng., **34** (6), 1558–1568 (1995). DOI: 10.1117/12.206161
[61] N. Ghosh, M.F.G. Wood, I.A. Vitkin. J. Biomed. Opt., **13** (4), 44036 (2008). DOI: 10.1117/1.2960934
[62] J. Song, N. Zeng, H. Ma, V.V Tuchin. IEEE J. Sel. Top. Quantum Electron., **29** (4), 1–9 (2023). DOI: 10.1109/JSTQE.2022.3197599
[63] D.H. Goldstein. Appl. Opt., **31** (31), 6676–6683 (1992). DOI: 10.1364/AO.31.006676
[64] Z. Chen, X. Chen, L. Tao, K. Chen, R. Zhang, M. Long, E. Pickwell-MacPherson, J. Xu. ACS Photon., **9** (11), 3633–3641 (2022). DOI: 10.1021/acsphotonics.2c01128
[65] X. Liu, X. Chen, E.P.J. Parrott, C. Han, G. Humbert, A. Crunteanu, E. Pickwell-MacPherson. APL Photon., **3** (5), 51604 (2018). DOI: 10.1063/1.5010940
[66] X. Liu, X. Chen, E.P.J. Parrott, E. Pickwell-MacPherson. Photon. Res., **5** (4), 299 (2017). DOI: 10.1364/PRJ.5.000299
[67] C. Han, E.P.J. Parrott, E. Pickwell-MacPherson. IEEE J. Sel. Top. Quantum Electron., **23** (4), 1–6 (2017). DOI: 10.1109/JSTQE.2016.2641581
[68] A.I. Hernandez-Serrano, Q. Sun, E.G. Bishop, E.R. Griffiths, C.P. Purssell, S.J. Leigh, J. Lloyd-Hughes, E. Pickwell-MacPherson. Opt. Express, **27** (8), 11635 (2019). DOI: 10.1364/OE.27.011635
[69] A.I. Hernandez-Serrano, D.M. Mittleman, E. Pickwell-MacPherson. Opt. Lett., **45** (5), 1208 (2020). DOI: 10.1364/OL.45.001208

Translated by D.Safin